A SIMPLE AND ACCURATE 3D NUMERICAL MODEL FOR LASER CLADDING

Shih-Kai Chien **Kuo-Teng Tsai**

Laser and Additive Manufacturing Technology Center
Industrial Technology Research Institute
Tainan, Taiwan

Yueh-Heng Li

Department of Aeronautics and Astronautics
National Cheng Kung University
Tainan, Taiwan

Yu-Ting Wu

Department of Engineering Science
National Cheng Kung University
Tainan, Taiwan

Wen-Lih Chen*

Department of Aeronautics and Astronautics
National Cheng Kung University
Tainan, Taiwan

ABSTRACT

A simple numerical model has been proposed for laser cladding. The model does not involve complex techniques such as cell addition, moving mesh, or prescribing a clad profile with a certain polynomial function. Instead, a mass function has been introduced to register the clad mass deposition on substrate, and from which the clad-track height can be estimated. The model takes several operational parameters, laser power, laser-head speed, and clad powder feeding rate, into consideration and predicts clad-track geometry, dilution, and substrate temperature. Experiments using two different combinations of substrate and clad powder materials to lay single and multiple clad tracks were conducted to provide data for model validation. The results show that the present model returns good agreement with experimental clad profiles for single and multiple tracks.

Keywords: laser cladding; numerical method; clad profile; dilution.

1. INTRODUCTION

Laser cladding (shown in Fig. 1) is an innovative machining method which deposits layers of clad material on a substrate to repair surface cracks or to create a protective coating. The cladding process can be achieved by either pre-placed powder or blown-powder methods. During this process, laser melts the surface of substrate and forms a melt pool. The powder is then injected into the melt pool by a co-axial or off-axial nozzle using inert carrier gas. As the powder exits the nozzle, it forms a powder stream which impinges on the same substrate-surface spot where the laser beam is irradiated. The powder is melted and captured by the melt pool, where both the powder material and the substrate material are mixed to form metallurgical bonding between coating and substrate when the melt pool is solidified. Inert gas such as argon, nitrogen, or helium is often used as carrier gas

* Corresponding author (wlchen@mail.ncku.edu.tw)

DOI : 10.1017/jmech.2019.30

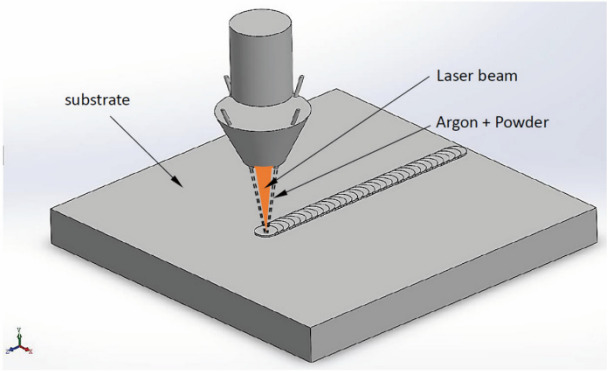

Fig. 1 Schematic of a laser cladding process.

which also serves to shield the melt pool against oxidation. As the laser beam and powder stream travel along the substrate surface, they leave a clad track behind. Such a track can be very thin; therefore, multiple tracks can be overlapped to form a thicker coating in practice. In laser cladding, the clad-track geometry is very important for the quality of finished product. If holes or cracks exist, the integrity of clad track will be compromised, and its mechanical properties to resist wear can be impaired. Dilution is another important factor determining the quality of the finished product. It is very important to find how clad geometry and dilution are affected by various operational parameters such as laser power, powder feeding rate, and laser-head speed.

The physical process of laser cladding is very similar to laser welding, both involving melting and solidification of metal by a high-energy-intensity heat source. Since the development of laser welding preceded laser cladding, early development in analytical or numerical techniques focused on laser welding. The numerical models for laser welding can be classified into heat-conduction-based models and convective-heat-transport-based models (Nguyen and Yang [1]). In heat-conduction-based models, only the solid domain is considered, and the heat source is approximated by some 2D Gaussian disk or 3D Gaussian conical profiles, for example, the work of Pavelic *et al*. [2], Goldak *et al*. [3], and Goldak [4]. On the other hand, convective-heat-transport-based models, for example the work of Ho and Kim [5] and De and DebRoy [6], further consider the molten phase, and more accurate geometry of melt pool can be predicted by taking the effects of heat convection in melt pool due to buoyance and thermocapillary forces into account. The former models are simple and computationally inexpensive. However, they require some ad-hoc calibration on some geometrical parameters for the heat source profiles to return accurate temperature solutions. The later models require much less, or almost no ad-hoc tuning to achieve accurate solutions, but they are numerically more complex and computationally time-consuming.

Many analytical and numerical models have also been proposed to study the effects of various parameters on laser cladding and the final clad geometries. Lalas *et al*. [7] developed an analytical model to predict laser clad geometry. The model assumed that a clad geometry is formed through two steps; step 1: to calculate the liquid clad volume per unit length by powder feeding rate, and step 2: to estimate the clad geometry based on liquefied clad and substrate. Factors such as powder feeding rate, laser speed, and surface tension between clad and substrate were considered. The model was demonstrated to return reasonable agreement with the data in terms of clad width and depth under low and medium process speeds. The numerical models for laser cladding can be classified in the same way as the laser welding models. In terms of conduction-based models, Toyserkani *et al*. [8] proposed a 3D finite element model to investigate the effects of laser pulse shaping on a powder-injection laser cladding process. The model considered parameters such as laser pulse shaping, travel speed, laser pulse energy, powder jet geometry, and material properties and could predict clad geometry. The concept was to decouple the interaction between melt pool and powder. Substrate was first calculated to establish the boundary of melt pool, then a layer of coating material was deposited on the overlapping area between powder stream and melt pool. The thickness of the deposited material was estimated according to powder feeding rate and elapsed time. A cell adding strategy was implemented to mimic the growth of clad thickness on the substrate. Finally, a new melt boundary was calculated based on the thermal and heat transfer analysis of deposited clad track, substrate, and laser power. The numerical results were compared with experimental data, and reasonable agreement with the data was obtained. Ya *et al*. [9] developed a 2D model to predict clad geometry during laser cladding. The model was based on laws of mass and energy balance. A parameter of special interest was the powder efficiency, and the changes in powder efficiency due to various clad conditions were studied. The model did not involve a liquid phase to simulate the behaviors of molten material and its interaction with powder; instead, a parabolic profile was adopted to prescribe the geometry of clad layer. The method allowed single as well as multiple clad tracks to be simulated. An algorithm to overlap multiple parabolic profiles was proposed to simulate multiple-track problems. However, one disadvantage of this approach is that parabolic profile is not a general profile for various clad tracks created under different conditions. That is, a clad profile should be predicted instead of being prescribed. Nevertheless, the study found that powder efficiency increased as input energy increased up to a certain level, and the increase in powder efficiency became marginal afterwards. However, the dilution continued to increase as energy increased within the tested energy level. Hofman *et al*. [10] reported a numerical and experimental study on dilution control in laser cladding. The numerical model was a finite element method. The clad geometry was calculated by a method based on substrate melt pool and powder mass that received by the melt pool, like the method proposed in Toyserkani *et al*. [8]. The results showed good degree of agreement between the prediction and experimental data. It was found that there existed a good correlation between melt pool width and dilution, making the former a good sensor for online dilution control. Palumbo *et al*. [11] investigated

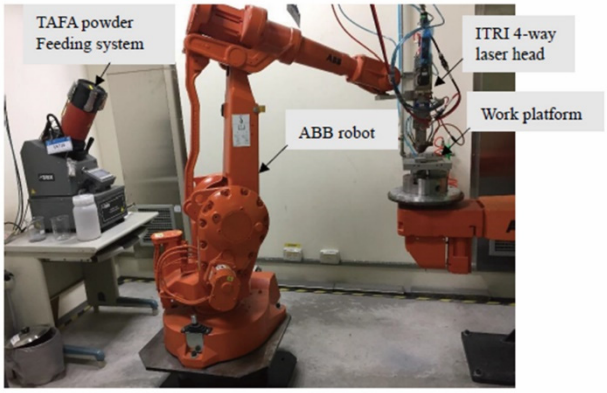

(a) Experimental setup.

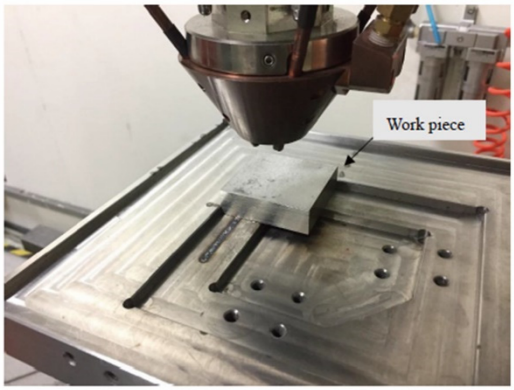

(b) Laser-cladding work platform.

Fig. 2 Experimental setup and the laser cladding work platform.

Fig. 3 The TRUMPF TruDisk 6002 laser used for the current laser-cladding experiment.

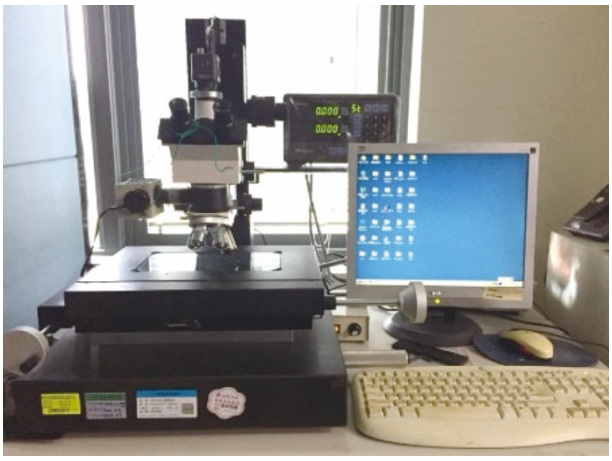

Fig. 4 KUNOH BK-03 electronic microscope.

thermal cycles, variations of dilution, and melt-pool shape during laser cladding on ring geometries. A 3D thermo-mechanical finite element model was used to predict temperature and stress distributions, and experimentally measured clad dimensions and profiles were adopted to prescribe clad geometries. In this method, clad cells were built into the numerical model at the beginning, and they were activated once the laser spot irradiated on them.

There have been very few convective-heat-transport models for laser cladding. Parekh *et al*. [12] studied the effects of several process parameters on clad geometry using a multi-physics simulation. The laser cladding process was to coat copper on a SS316L substrate using a CO_2 laser. The interaction between solid and molten phases was modelled using volume of fluid (VOF) and moving mesh, hence a commercial package COMSOL was employed to deal with the complex numerical treatment. Since the mathematical model was rather complete, it could predict temperature distributions, stress conditions, dilution, and clad geometry. Several findings were reported including the effects of laser power, travel speed, laser-spot diameter, and powder flow rate on clad geometry. However, no comparison with experimental data was given.

The above numerical laser-cladding models incorporated some techniques such as cell addition, pre-built-in cells, VOF, or moving mesh to deal with the growing process of clad track on substrate. These techniques are sources of numerical complexity which results in difficulty in coding and prolonged simulation time. Furthermore, for those models excluding liquid phase, clad geometry was often prescribed, making the prediction lack of generality in single-track cases and very difficult in multiple-track cases. Liu and Li [13] proposed a model to estimate clad profile based on clad height. The clad height was determined by the clad mass accumulation on substrate surface which was estimated by a Gauss distribution function and the interaction time between laser spot and substrate surface. In this model, effects from surface tension, gravity, and gas flow on clad formation were arguably too small and were neglected, and there was no thermal model involved; hence only the clad profile could be predicted. The major advantage of this model is that there is no need to involve a prescribed polynomial for clad profile. However, the model was only tested to predict single-track clad profiles.

The objective of this study is to develop a simple heat-conduction-based model with minimal empirical specifications and yet accurate enough for single- as

well as multiple-track laser cladding predictions. The concept of Liu and Li [13] has been adopted, hence the present model is free from using any prescribed function for predicting clad profiles. The model can predict clad geometry, dilution, and temperature distributions of the substrate without involving mesh addition or moving mesh. Effects of powder efficiency and substrate absorption rate are taken into consideration. The final clad geometry is a function of several operational parameters including laser power, laser-head speed, and powder feeding rate.

2. EXPERIMENTAL SETUP

The experimental setup, including laser, laser head, robot arm, powder feeding system, work platform, is shown in Fig. 2. In this setup, the laser head is driven by the robot arm. The clad powder is delivered to the laser head by a piping system, and the laser beam is transmitted to the laser head through an optic fiber. Fig. 3 shows the laser, which is a TRUMPF TruDisk 6002. It is a solid-state disk laser design for welding, cutting, and surface processing of metals. The wave length of the laser beam is 1064 nm, while the laser-beam diameter can be adjusted within a range from 0.003 m to 0.0035 m. The maximum laser power is 6 kW, and the accuracy on laser-power control is within 1%. The laser head is an inhouse 4-way laser head developed by ITRI. Its movement over the work platform is driven by an ABB robot. The ABB robot can operate within a working space of 1m× 1m× 1m and achieve laser-head speed accuracy within 1%. In this study, two combinations of substrate and clad powder materials have been tested. In one combination, the substrate is SUS 304 stainless steel, and the powder material is Inconel 718; and in the other combination, the substrate is 6061 aluminum alloy, and the powder material is A356 aluminum alloy. A TAFA Model 1264i powder feeding system is feeding powder to the laser head, and the feeding rate accuracy is within 2.4%. Argon gas blown at a fixed flow rate of 0.1333 Ls^{-1} is used as the protecting gas for the powder. This setup can accurately control important operational parameters affecting clad track quality such as laser power, powder feeding rate, and laser-head speed, to produce reliable data for the validation of the proposed numerical model. After laser cladding, a work piece can be cut and polished to reveal the clad-track geometry. The cut work piece is then placed under a KUNOH BK-03 electronic microscope shown in Fig. 4 for the measurement on the dimensions of the coated clad profile.

3. MATHEMATICAL MODEL

To simplify the numerical procedure for laser cladding, the following assumptions are made:

- The substrate is fixed, and the laser spot and powder stream are moving during laser cladding; hence a fixed coordinate system is used for the numerical analysis.
- The vertical distance between laser head and substrate surface is fixed, and laser energy absorption by the substrate only happens at the location on substrate surface that is covered by the laser spot.
- The heat loss of powder particles via convection and radiation is not considered because of the short-time interaction between powder and laser.
- As powder particles reach the substrate surface, their temperature is the same as the substrate temperature.
- Attenuation of laser energy due to the blockage of powder particles is not considered since powder particles which carry the laser energy they obtained by obstructing it from reaching the substrate surface will eventually reach substrate surface and transfer such energy to the substrate.
- The heat convection inside the melt pool is neglected; hence thermal analysis is only implemented on substrate where only solid phase is considered. This is so called heat-conduction based analysis. The effects of melt pool and powder deposition on substrate are taken into account by modifying substrate's material properties such as specific heat, thermal conduction, and density.

Since only the substrate is meshed and solved numerically, the mesh remains the same at all time. The clad track is represented by a mass function and a thickness function defined on the substrate surface on which the powder material has been deposited. The effects of clad mass and temperature are considered by modifying the density and physical properties of those substrate cells at which the clad track is situated. Thermal properties of substrate are functions of temperature. Sistaninia *et al*. [14] classified the governing equations for problems involved moving laser heat source into Eulerian and Langrangian formations. The Eulerian formation gives rise to a steady-state governing equation; whereas, the Lagrangian formation results in a transient governing equation. In this study, the beginning and the ending stages of laser cladding are simulated, hence it is a transient problem. In this case, only the Langrangian formation is suitable for the current study. To this end, the transient energy equation can be expressed as:

$$\rho_{eff} C_{eff} \frac{\partial T}{\partial t} = \nabla\left(\lambda_{eff} \nabla T\right) \tag{1}$$

where ρ_{eff}, C_{eff}, and λ_{eff} are respectively the effective densities, specific heat, and thermal conductivity of the substrate. Note that there is no convection term in equation (1) because fixed coordinate system is adopted.

If no clad is deposited on a substrate cell, its effective density is equal to substrate density, which is a function of temperature. If there is clad deposited on a substrate cell, its density is calculated by:

$$\rho_{eff} = \frac{m_s + m_c}{V_{cell}} \tag{2}$$

where m_s and m_c are respectively the masses of substrate and clad deposition on that cell. Since the molten liquid state of substrate is not simulated, the effect of latent heat of fusion is approximated by increasing specific heat:

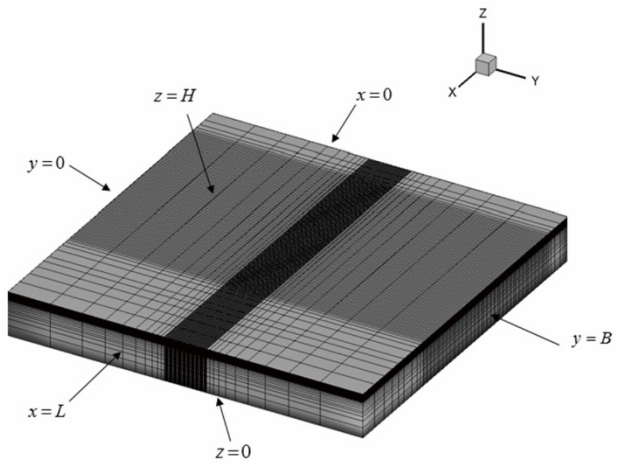

Fig. 5 Computational mesh for single-track cases.

$$C_{eff} = \frac{L_f}{T_m - T_s} + C_s \tag{3}$$

where L_f, T_m, T_s, and C_s are substrate's latent heat of fusion, melting temperature, solidification temperature, and specific heat, respectively. The effective thermal conductivity is substrate's thermal conductivity in the case of no clad deposition. For the case of clad deposition, it is weighted between the thermal conductivities of substrate and powder material via their mass fractions:

$$\lambda_{eff} = f_s \lambda_s + (1 - f_s)\lambda_p \tag{4}$$

where f_s, λ_s, λ_p are substrate mass fraction, substrate thermal conductivity, and powder material thermal conductivity, respectively.

The geometry of laser cladding is strongly affected by temperature distribution, which, in turn, is determined by Q_{abs}. The substrate is assumed to be at a constant initial temperature. On the substrate surface on which laser spot is irradiated, the laser intensity profile $I(x, y)$ is a Gaussian profile:

$$I(x,y) = \frac{2P_l}{\pi R_l^2} \exp\left\{ \frac{-2\left[(x - x_l)^2 + (y - y_l)^2 \right]}{\pi R_l^2} \right\} \tag{5}$$

where P_l is laser power; R_l is laser beam radius; (x_l, y_l) are the coordinates of the laser-spot center. Note that laser spot center will move during laser cladding, hence (x_l, y_l) are functions of time. The absorbed heat power by a surface cell located at (x, y) on substrate surface is:

$$Q_{abs}(x,y) = \gamma I(x,y) \Delta A \tag{6}$$

where γ is the absorption coefficient of the substrate, and ΔA is the surface area of the cell.

In this model, energy loss is mainly due to natural convection on substract surfaces and thermal radiation at high temperature regions. Rate of heat loss due to natural convection can be expressed as:

$$Q_{nc} = -h_{nc}(T - T_0) \tag{7}$$

where T_0 is ambient temperature. Equation (7) is applied to x=0, x=L, y=0, and y=B shown in Fig. 5. During laser cladding, natural convection as well as thermal radiation occur on the high-temperature cladded area. Goldak [4] and Yang *et al*. [15] proposed a combined heat transfer coefficient to approximate the rate of heat loss:

$$Q_{loss} = -h_{combined}(T - T_0) \tag{8}$$

$$h_{combined} = 24.1 \times 10^{-4} \varepsilon_t T^{1.61} \tag{9}$$

The value of ε_t depends on substrate material, and it is 0.9 for stainless steel. Equation (9) is applied to z=H shown in Fig. 5. Finally, adiabatic condition is applied to z=0 at the bottom of the substrate.

The shape of clad track is strongly affected by the radius of laser beam, melt pool, and powder deposition. The melt pool size is determined by laser energy absorbed by the substrate. Since clad track is an interaction between powder stream and melt pool, the final clad track geometry can be calculated by the integration of powder feeding rate over the melt pool within the interaction time. The clad mass accumulated on a cell with cell center coordinates (x, y) can be expressed as:

$$m_c(x,y) = \int_{t_1}^{t_2} \eta \dot{m} A(x,y)\, dt \tag{10}$$

where η is powder efficiency, $\dot{m}$ is powder mass flow rate per unit area, $A(x, y)$ is the surface area of the cell; t_1 and t_2 are respectively the beginning and ending of the time when the cell is molten and is within the powder stream. After the clad mass function $m_c(x,y)$ being established on substrate surface, clad height on substrate surface can be estimated by:

$$H_c(x,y) = \frac{m_c(x,y)}{A(x,y)\rho_c} \tag{11}$$

where ρ_c is the density of clad, and $A(x,y)$ is the surface area of the cell with cell-center coordinates of (x,y). One great advantage of this method is that there is no need to specify a clad geometry.

4. NUMERICAL APPROACH

An inhouse CFD code, "USTREAM", developed by the corresponding author has been modified to perform the computation in this study. This is an unstructured-mesh, fully collocated, finite-volume code descended from a structured-mesh multi-block code "STREAM" developed by Lien *et al*. [16]. Since there is no fluid domain in the present model, only the energy equation in UNSTREAM is activated. Some additional subroutines

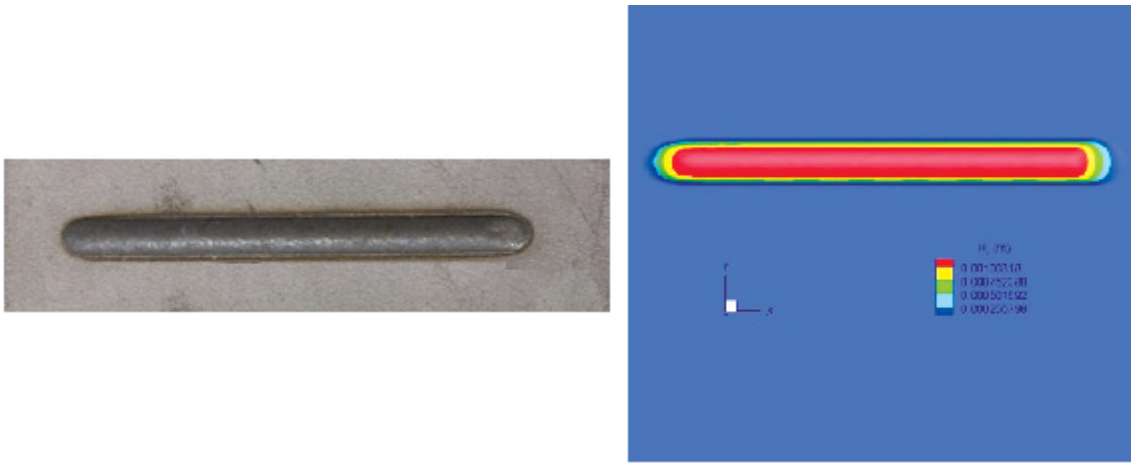

(a) Experimental clad track (b) Numerical clad track

Fig. 6 Top-view of the experimental and numerical clad tracks produced by laser power of 2,000 W.

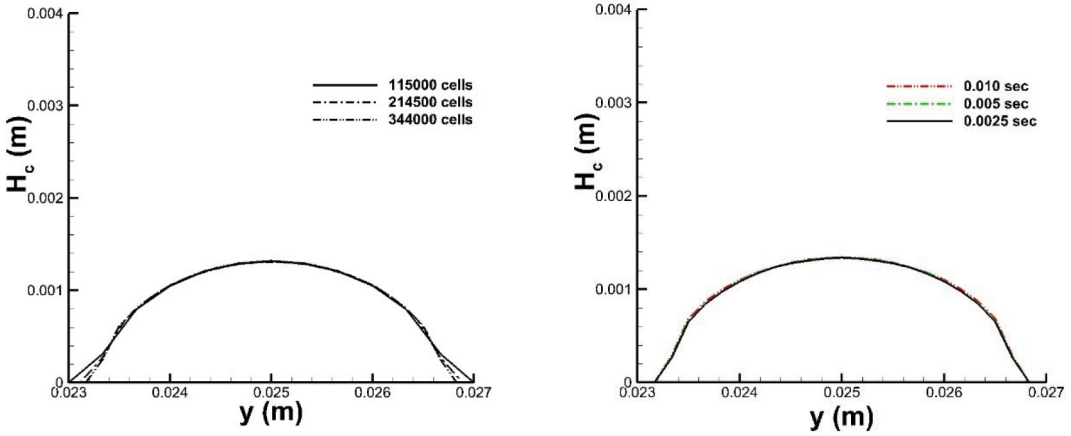

(a) (b)

Fig. 7 Comparison of clad profiles at 2,000 W laser power obtained by (a) three different meshes with cell numbers of 115,000, 214,500, and 344,000, and (b) three different time step intervals of 0.01, 0.005, and 0.0025 sec.

are added to calculate clad mass and clad height using equations (10) and (11), respectively.

5. RESULTS AND DISCUSSION

The first step of numerical simulation is to determine a proper mesh and time-step interval to obtain grid- and time-step-interval-independent solutions. A test case laying an Inconel 718 clad track on a SUS 304 substrate is adopted for this task. Tabulated values of temperature dependent thermal properties, $\rho_s(T)$, $C_s(T)$, and $\lambda_s(T)$ of SUS 304 and Inconel 718 in Mills [17] are used. Latent heat, melting temperature, and fusion temperature of SUS 304 are 227 kJkg^{-1}, 1,610 K, and 1,568 K, respectively. A reasonable absorption rate of 0.3 is set for SUS 304. In the grid-independent test, the substrate's length, width, and height are L=0.05 m, B=0.05 m, and H=0.015 m, respectively. The initial substrate temperature is 300 K, and the laser power is 2,000 W. Three meshes with cell numbers of 115,000, 214,500, and 344,000 have been examined. Fig. 5 depicts the 214,500-cell mesh. Note that cells are concentrated towards top surface and the area where clad track will be laid. The laser-spot velocity is 0.011 ms^{-1}, and the time step interval is fixed at 0.005 sec. Top views of the experimental and computational clad tracks are shown in Fig. 6. The comparison between experimental and numerical clad tracks will be given later in Subsection 5.1. Here, the picture is only for explaining how a clad-track profile is measured. The picture shows that the clad-track geometry begins with a short developing (transition) section where clad height gradually increases. This is followed by a uniform, steady-state section with constant clad height. Towards the end of the track, the clad height gradually declines to zero in the other short transition section. A clad profile is measured (or taken) from a certain cross-section cut in the steady-state section. The clad profiles returned by the three meshes are given in Fig.7 (a). The picture shows that all profiles are almost the same except some small differences

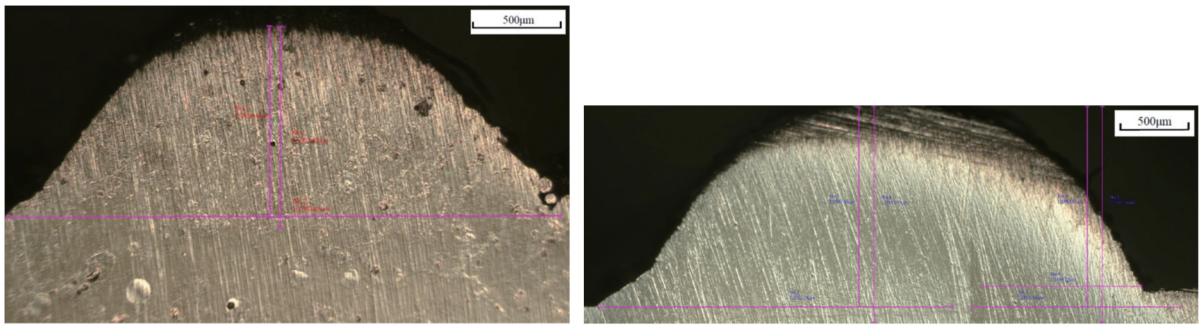

(a) 750 W (b) 1,500 W

Fig. 8 Photographs of clad-track-cross-section cuts produced by laser power of 750W and 1,500 W.

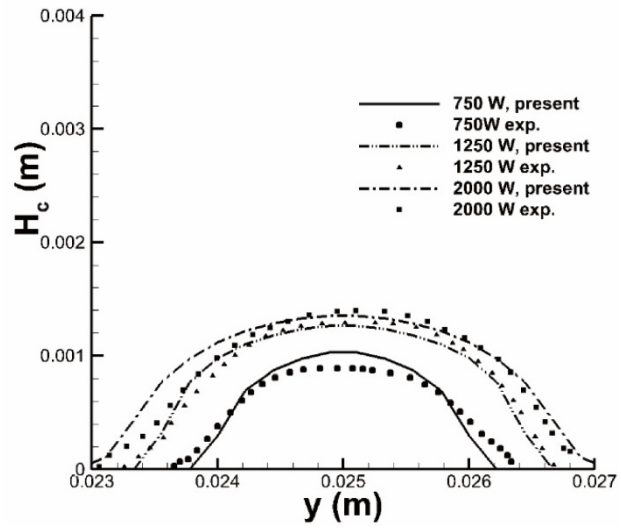

Fig. 9 Comparison of clad profiles between present method and experiment at three different laser power levels, 750 W, 1,250 W, and 2,000 W.

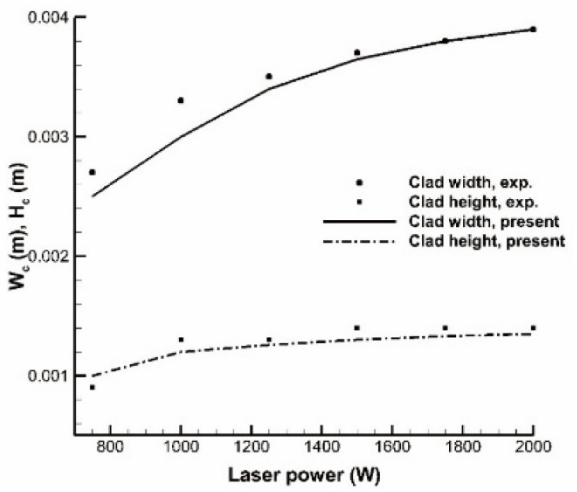

Fig. 10 Comparison of clad width and height between experiment and the present method under various laser power levels.

at the two profile edges. Among them, the medium- and fine-mesh profiles are almost identical even at these edges. This test indicates that the medium mesh is fine enough to produce grid-independent solutions, and it is used for the rest of single-track cases in this study. A different mesh with similar cell density to that of the medium mesh is adopted for multiple-track cases. Another test with the medium mesh and three time-step intervals of 0.01, 0.005, and 0.0025 sec was conducted to determine a proper time-step interval, and the results are shown in Fig. 7 (b). It was found that the clad profile exhibits very little sensitivity to these different time-step intervals. Hence, the medium time-step interval was selected for this study.

1.1 Single track – Inconel 718 on SUS 304

In the first group of single-track cases, Inconel 718 tracks are laid on SUS 304 stainless steel substrates. The operation conditions are as follows: laser beam radius is 0.00175m; laser head speed is 0.011 ms^{-1}; powder feeding mass flow rate is 2.73×10^{-4} kgs^{-1}; powder efficiency is assumed to be 0.9; laser power levels are 750 W, 1,000 W, 1,250 W, 1,500 W, 1,750 W, and 2,000 W. The substrate dimensions are the same as those stated in the grid-independence test. Natural convection coefficient on substrate surface is assumed to be 10 $Wm^{-2}K^{-1}$. The laser center was initially positioned at the coordinates of (x, y) = (0.01 m, 0.025 m) and traveled 0.035 m along x direction. From Fig. 6, it is noticeable that the numerical clad-track geometry resembles the experimentally observed geometry quite well. The experimental clad-track geometry consists of a uniform, steady-state section and two semi-circular transition sections located respectively at its two ends. Between the two transition sections, the slope at the front transition section is steeper than the other one at the rear. These important geometrical features are very well captured by the numerical model. Experimental

cross section cuts of clad track produced by laser power levels of 750 W and 1,500 W are given in Fig. 8. The experimental clad profiles were measured from cross section cuts such as this. Fig. 9 shows the comparison of clad profiles at three different laser power levels, namely 750 W, 1,250 W, and 2,000 W. It can be noted from Figs. 8 and 9 that clad profiles, no matter produced by high or low laser power levels, are similar in shape and are more

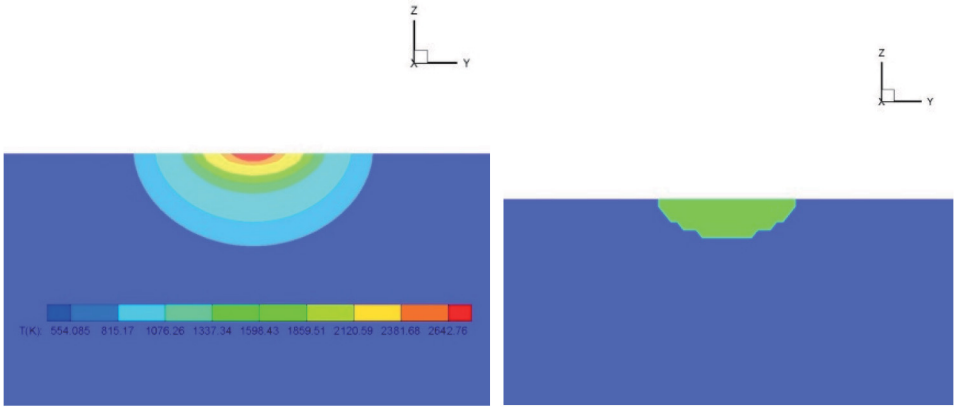

(a) Temperature contours. (b) Melt pool size.

Fig. 11 Substrate temperature contours and molten pool size of the cross section at x = 0.025 m and t = 1.37 sec in the case of 1,000 W laser power.

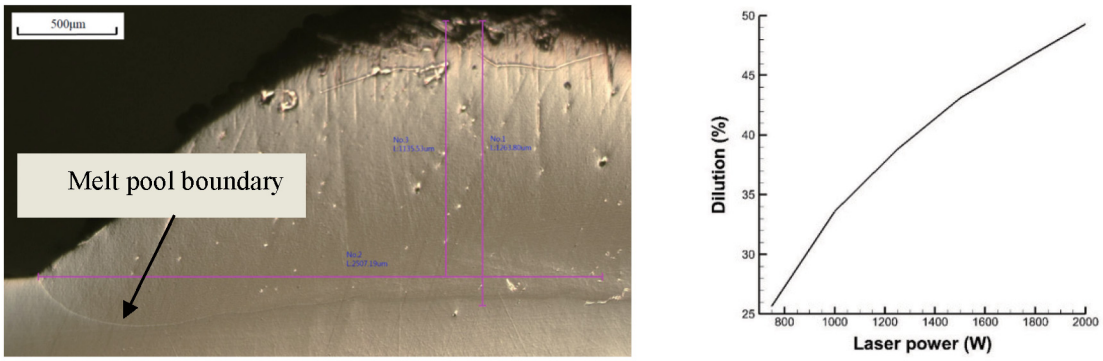

(a) Experimental melt pool. (b) Dilution versus laser power.

Fig. 12 Experimental melt pool profile and the effects of laser power on dilution.

or less symmetrical to the coordinate of laser spot center at y = 0.025 m. By focusing on the left half of a typical clad profile, it can be observed that the profile generally curves upwards near the left edge and curves downwards near the center, suggesting the existence of an inflection point in between. Hence, the profile curve must be at least a cubic or higher order polynomial. This implies that the approach of prescribing a parabolic clad profile suggested by Ya *et al*. [9] is not applicable to those cases in this study. Fig. 9 in Hofman *et al*. [10] shows four different clad profiles produced by different laser power levels and laser spot speeds reported. There are two profiles resemble parabolic curves, whereas the other two profiles clearly do not. The above results and those reported in Hofman *et al*. [10] prove that clad profiles will not always follow a certain polynomial function under different conditions. Hence, prescribing a clad profile by using a specific function cannot be a general practice for different laser cladding processes.

Fig. 9 shows that the present model returns profiles which are qualitatively and quantitatively in good agreement with the experiment. The predicted profiles capture experimental profile curves very well with only marginal derivations. Note that no prescribed polynomial function has been used in the present model. The clad profiles are the result of mass accumulation due to the interaction between melt pool and clad powder stream. The degree of good agreement is further confirmed in Fig. 10 where the comparison in clad width and height under various laser power levels is given. The growth rates for both clad width and height are higher at lower laser power but are lower at higher laser power, and the clad height seems to asymptotically approach a value of 0.0014 m. In terms of clad width, its growth becomes marginal as it becomes larger than the laser-spot diameter. This is because the width of substrate's melt pool can only grow slightly larger than the laser-spot diameter (0.0035 m). Such behaviors are consistent with the observations reported in Hofman *et al*. [10]. The model slightly underestimates clad height in general, but the differences are all within 5%. In terms of clad width, the model returns slightly shorter clad width under lower laser-power conditions; but the prediction improves under higher laser-power conditions. For example, the predicted width is almost identical to measurement at laser power levels of 1,750 W and 2,000 W. The reason for the underestimation on clad-track width could be due to that some molten powder particles can still stick to the adjacent area to the melt pool edge, making the clad-track wider. On the other hand, the numerical model only allows powder

Table 1 Test conditions in group 2.

Case No.	Laser power (W)	Scanning speed (ms^{-1})	Power feeding rate (kgs^{-1})
1	2,000	0.015	0.000216
2	2,400	0.007	0.000273
3	2,000	0.011	0.000273
4	1,600	0.011	0.000216
5	2,400	0.015	0.000273
6	2,400	0.011	0.000216
7	1,600	0.015	0.000273
8	1,600	0.011	0.000328
9	2,400	0.011	0.000328
10	2,000	0.007	0.000328
11	2,000	0.007	0.000216
12	1,600	0.007	0.000273
13	2,000	0.015	0.000328

particles to deposit inside the melt pool, and those particles outside the melt pool pose no effect in forming clad coating.

One of the important quantities for the quality of laser cladding is dilution. Some degree of dilution is needed to create a strong bond between clad layer and substrate, but excessive dilution is not desirable because this will lead to a large heat-affected zone, which in turn could compromise the quality of the finalproduct. Dilution is defined as:

$$D_c = \frac{A_m}{A_m + A_c} \times 100\% \tag{12}$$

where A_m and A_c are respectively the cross-section areas of molten substrate and clad track measured from a cross section. In the numerical model, dilution can also be estimated using volumes of molten substrate and clad track:

$$D_c = \frac{V_m}{V_m + V_c} \times 100\%, \tag{13}$$

where V_m and V_c are respectively the volumes of the substrate that has once been molten during laser cladding and of the clad track. Fig. 11 (a) shows the cross-section temperature contours at $x = 0.025$ m of the case with 1,000 W laser power at $t = 1.37$ sec. At this moment, the laser spot center has traveled to the location of $x = 0.025$ m. A flag is set to unity in a cell once its temperature is higher than the melting temperature. Fig. 11 (b) shows those cells whose flag has been set to unity at this cross section. At the end of simulation, V_m in equation (13) is calculated by integrating the volume of all cells whose flag has been set to unity.

Measuring dilution requires dedicated software to analyze digital images of melt pool in real time (Hofman, [18]). Since we don't possess similar software and imagining equipment, this quantity is approximated by using the height of clad track and the depth of the melt pool:

$$D_c \cong \frac{H_m}{H_m + H_c} \times 100\% \tag{14}$$

Unfortunately, as shown in Fig. 12 (a), a typical melt pool boundary in this group of cases is rather irregular, making such estimation inaccurate. Hence, only the simulated results are given here. In Fig. 12 (b), dilution increases as laser power is increased. The increase rate is higher when laser power is low, and it slightly decreases when laser power is high. The results highlight the disadvantage of using high laser power which tends to create a larger heat-affected zone.

1.2 Single track – A356 on 6061

In the second group of single-track cases, clads of aluminum alloy A356 are laid on a substrate of aluminum alloy 6061. Again, tabulated temperature-dependent thermal properties in Mills [17] are used for the 6061 alloy. There are 13 cases in this group, and the test conditions are listed in Table 1. In this experiment, there were three laser power levels, 1,600, 2,000, and 2,400 W, three laser-head scanning speeds, 0.007, 0.011, and 0.015 ms^{-1}, and three power feeding rates, 0.000216, 0.000273, and 0.000328 kgs^{-1}. However, not all possible combinations of these three parameters were tested. Fig. 13 shows clad cross-sections of cases 3, 6, and 10. It is noticeable that experimental clad profiles are not always symmetrical, and one or two small irregular lumps of protrusions randomly appear on the profiles of some cases. These random protrusions could be due to some imperfection on the control of experimental conditions. For example, the powder particles cannot be perfectly homogeneously distributed inside the powder stream at all time, and there exists some minor fluctuations on the powder-feeding rate.

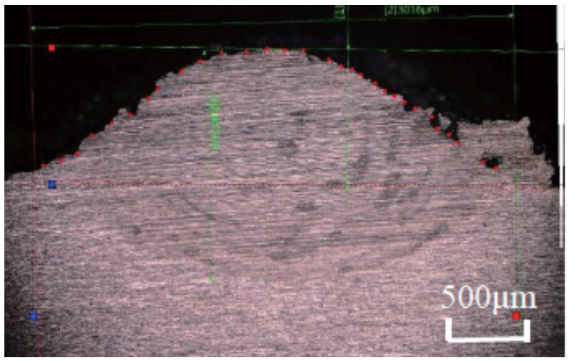

(a) Case 3.

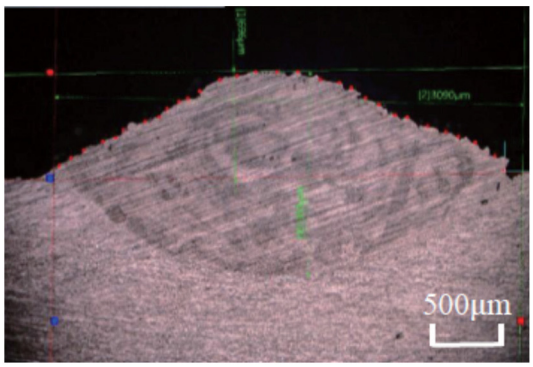

(b) Case 6.

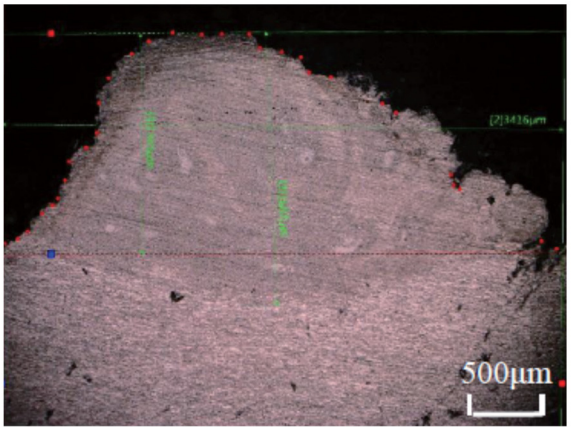

(c) Case 10.

Fig. 13 Group 2 clad-track cross-section cuts of cases 3, 6, and 10.

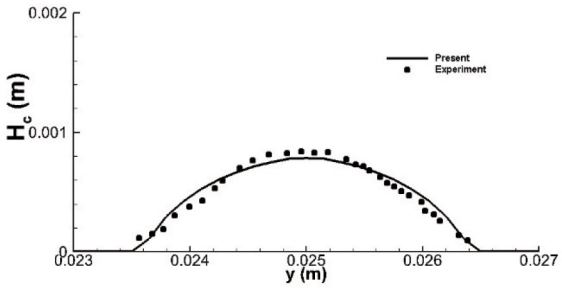

(a) Case 3.

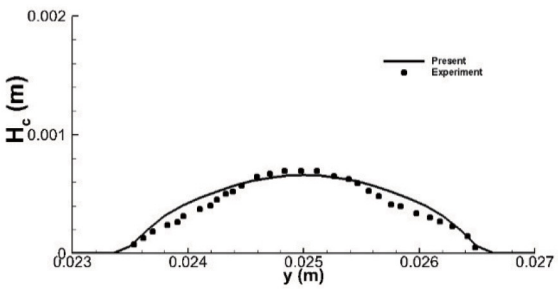

(b) Case 6.

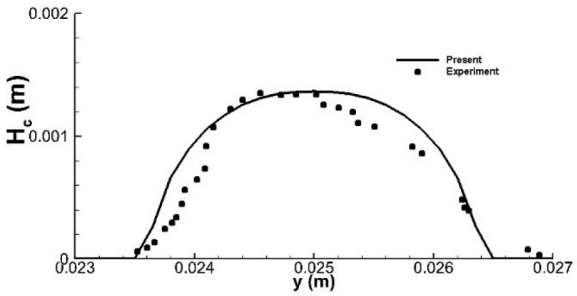

(c) Case 10.

Fig. 14 Comparison of Group 2 clad profiles of cases 3, 6, and 10.

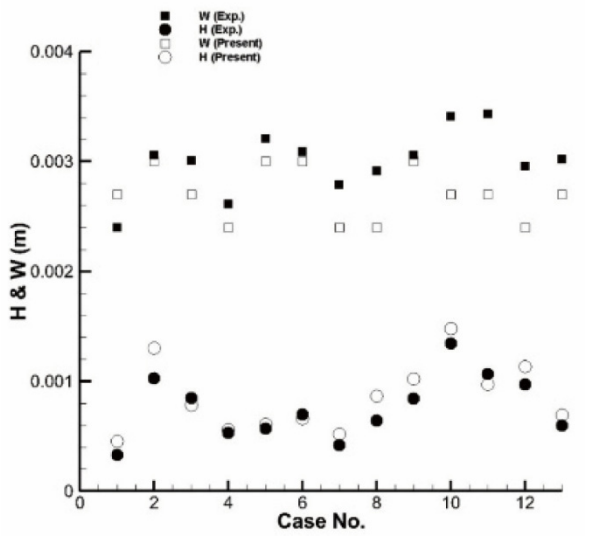

Fig. 15 Comparison of Group 2 experimental and numerical clad width and height.

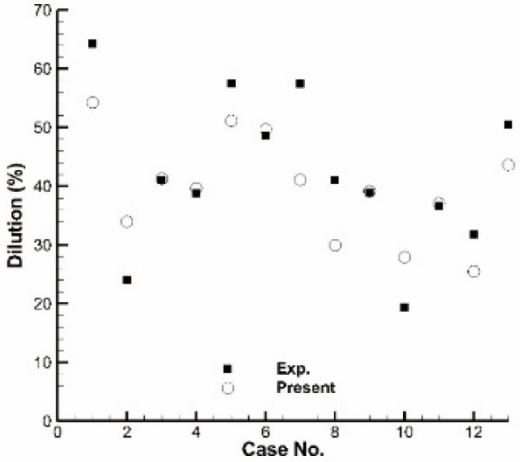

Fig. 16 Comparison of Group 2 experimental and numerical dilution.

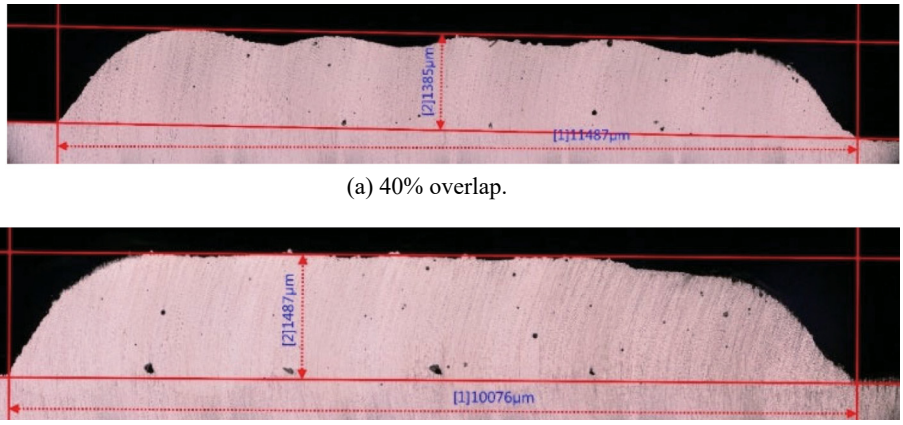

(a) 40% overlap.

(b) 50% overlap.

Fig. 17 Photographs of cross sections of multiple-clad-track cases.

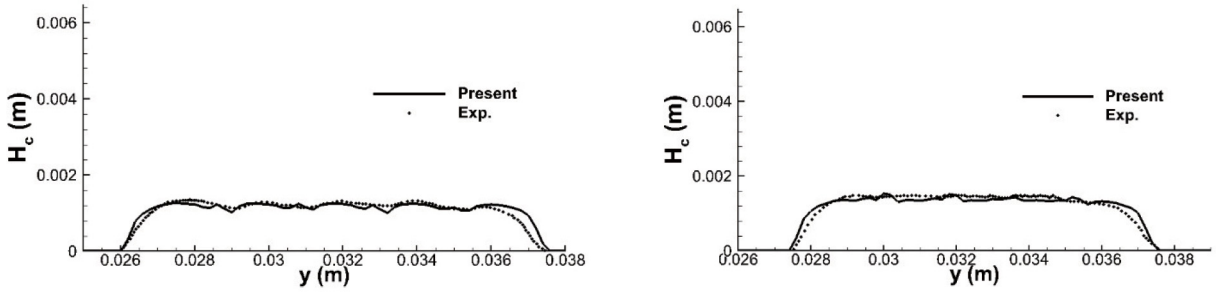

(a) 40% overlap.

(b) 50% overlap.

Fig. 18 Comparison between experimental and computational multiple track profiles.

Or, some gas flow effects such as evaporation that can push some material outwards may play a role. If these random protrusions are ruled out, the clad profiles are indeed quite symmetrical for most cases. This is reflected in Fig. 14 where experimental and numerical profiles are compared. As seen, the profiles of cases 3 and 6 are quite symmetrical; however, the profile of case 10 is clearly asymmetrical. This suggests that the level of experimental uncertainty tends to increase under high laser power, low scanning speed, and high powder feeding rate. Fig. 14 also indicates that the simulated profiles agree with experimental profiles reasonably well, especially for case

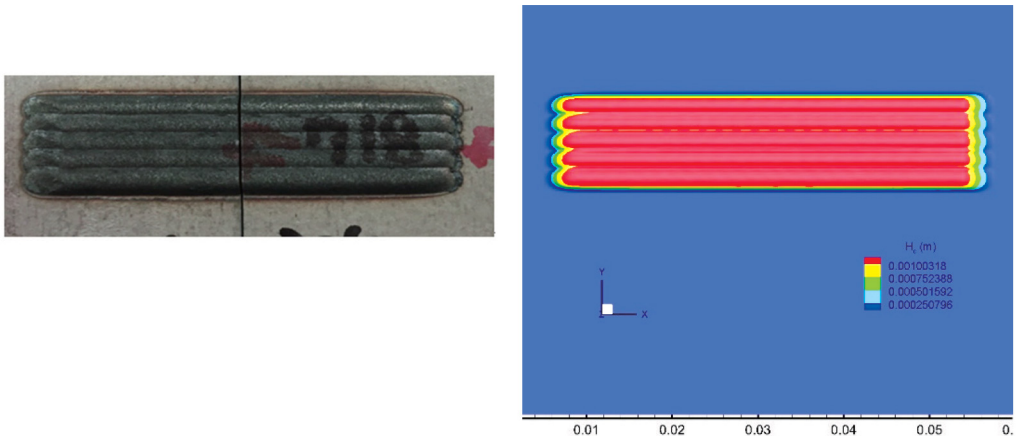

(a) Experiment. (b) Computational.

Fig. 19 Top view of multiple tracks of the case with 40% overlap.

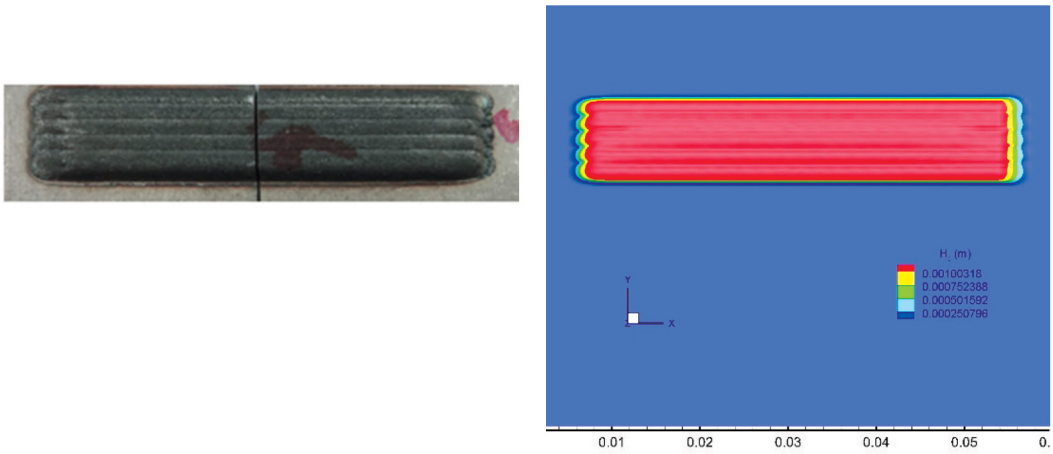

(a) Experiment. (b) Computational.

Fig. 20 Top view of multiple tracks of the case with 50% overlap.

3 and 6. The level of accuracy of the present method can be better understood from the comparison of clad width and height illustrated in Fig. 15. The figure indicates that the agreement between the model and experiment is quite good in general, especially in terms of the prediction on clad height. But there are larger discrepancies in clad width in some cases, for example, cases 8, 10, 11, 12. It can also be noted that the present method tends to underestimate clad width due to the same reason mentioned in the previous subsection.

As seen in Fig. 13, the melt lines on the substrate are quite regular, allowing accurate estimation on dilution. The comparison between simulated and experimental dilutions is given in Fig. 16. The agreement is reasonably good in most of the cases. However, there are larger discrepancies in cases 1, 2, 7, 8, and 10. The maximum discrepancy in terms of the dilution magnitude is 16 % in Case 7, but the discrepancies in the rest of cases are less than 10%. Case 3 has been experimentally executed five times, and the maximum and minimum dilutions are respectively 48% and 39%, giving rise to a maximum difference of 9% among these five experiments. This suggests that experimental uncertainty in dilution magnitude could be as high as 9%. Taking this magnitude of experimental uncertainty into consideration, the level of the discrepancies between numerical with experimental dilutions in Case 7 is not as bad as it appears to be.

1.3 Multiple-track cases

In this group of cases, the substrate and powder materials are the same as those in the first single-track group. However, the substrate length is now 0.1 m, which is twice the length of that in the single-track cases. Laser power was fixed at 1,250 W, and laser head speed was 0.011 ms^{-1} when laying clad tracks. The laser head was initially positioned at a higher y coordinate, then it was shuttled five times along the x-direction to lay five tracks. The laser spot traveled 0.05 m to lay each track, and it took one second for the laser head to reposition to the next starting point, which was located at a lower y coordinate than the previous one. Two cases have been conducted in this group; one was a 40% overlap, and the other was a 50% overlap. Here, “overlap” means the percentage of the overlap between laser spot radii of two adjacent clad

tracks. The distances between two adjacent clad tracks are respectively 0.00210 m, and 0.00175 m for 40% and 50% overlaps. Fig 17 illustrates the cross sections of the multiple clad tracks obtained in those two overlap conditions. As powder streams that create two adjacent clad tracks overlap more, clad material tends to pile up to gain more track height. But the overall clad-track width will be reduced due to the reduction in the distance between two adjacent tracks. As expected, the clad-track profiles in Fig. 17 indicates that the case with 50% overlap does produce higher clad height, meanwhile the clad top surface becomes more even. The clad heights are 0.001385 m and 0.001487 m respectively for cases of 40% and 50% overlaps.

Since the present model does not include a molten liquid phase, the physical process of melting the previous older clad track's material and mixing it with the newer track's material within the overlap region will not be simulated. However, a clad-mass-redistribution function has been introduced to modify the clad mass of the old track inside the overlap region to account for the effects of re-melting and mixing of old-track and new-track materials. To keep the algorithm simple, the mass function of the new track is not changed under this framework. The proposed clad-mass-redistribution function is a function of track-center distance between old and new tracks y_{dis} and the distance to the mid-point of the overlap region y_m. After calibrating with the experimental clad profiles, this function can be written as:

$$m_{c\_\text{modified}}(x,y) = m_c(x,y)\left\{1 - f_0 \exp\left[-\left(\frac{f_1(y-y_m)}{y_{dis}}\right)^2\right]\right\} \tag{15}$$

where y_m is the middle coordinate of old and new clad centers, $y_m = \frac{1}{2}(y_{c\_old} + y_{c\_new})$; y_{dis} is the distance between old and new clad centers; f_1 and f_2 are two factors defined as:

$$f_0 = 0.8; \quad f_1 = \begin{cases} 5, & y \geq y_m \\ 0, & y < y_m \end{cases} \tag{16}$$

The comparison between numerical and experimental multiple-track profiles is given in Fig. 18. Again, the model returns profiles which are in very good agreement with the experimental profiles for both cases. It is noticeable that width and height of the clad profiles as well as the profile curves are all well captured by the model. Especially the predicted width and height of the overall clad track are almost identical to the measurements. Figs. 19 and 20 depict respectively the top views of the experimental and the numerical clad tracks of 40% and 50% overlaps. These figures show that the simulated clad tracks look very similar to the experimental clad tracks. A typical multi-clad-track block features flute structures at the two ends, and the width of the first four tracks is much narrower than that of the fifth track due to partial track overlap. The track overlap phenomenon is more pronounced in the case of 50% overlap; hence the width of its first four tracks is even narrower. These features have been well captured by the numerical model, further proving the fidelity of the present model.

The dilutions of the 40% and 50% overlaps are 32.5% and 31.1%, respectively. The dilutions of multiple-track cases are smaller than that of single-track cases under the same laser power. This is expected because the laser spot of the current track re-melts a portion of the area that had been molten by the laser spot of the previous track. Hence, the overall molten volume in the substrate is reduced.

6. CONCLUSIONS

A simple heat-conduction based numerical model has been developed to simulate laser cladding. This model only solves the substrate domain. No complex techniques such as cell addition or moving mesh are involved. Instead, substrate's thermal properties are modified to account for temperature variation, melting and solidification of substrate material as well as the accumulation of clad material on substrate surface. A clad mass function is introduced to register clad mass deposition, and clad height can be estimated based on the clad mass function; hence the proposed model does not require any ad-hoc specification on clad profile. The model has been validated against single- and multiple-track experiments which include three groups of test cases. Groups 1 and 2 are single-track experiments, whereas group 3 is a multi-track experiment. Group 1 uses SUS 304 as substrate and Inconel 718 as clad powder; group 2 uses 6061 aluminum alloy as substrate and A356 aluminum alloy as clad powder; and group 3 uses the same materials as those in group 1. In single-track test cases, the model returns good agreement with experimental measurements in terms of clad-track geometries for different combinations of substrate and clad powder materials. The errors in terms of clad height and clad width are within 5% and 10% respectively in group-1 and group-2 cases. These results have verified general applicability of the model to different combinations of clad and substrate materials. The model can also predict dilution which is an important piece of information for the quality control on limiting heat-affected zone. In group 3, the numerical results have been validated against two cases with laser-spot radii overlap of 40% and 50%. A mass redistribution function has been introduced to account for the effects due to the process of re-melting of an old track and mixing with a new track. Again, the model returns very good agreement with the measured clad profiles in these two cases. These tests prove that the current simple model is accurate enough to assist the design of manufacturing processes involving laser cladding.

ACKNOWLEDGEMENTS

This work was supported by Industrial Technology Research Institute in Taiwan. The authors are very grateful for the financial support.

NOMENCLATURE

A surface area (m^2)
B substrate width (m)
C constant pressure specific heat ($kJkg^{-1}K^{-1}$)
C_M clad mass (kg)
D_c dilution
f mass fraction
f_0, f_1 factors in mass redistribution function
H substrate height (m)
H_c clad height (m)
h convective heat transfer coefficient ($Wm^{-2}K^{-1}$)
I laser intensity profile (or function)
L substrate length (m)
L_f latent heat of fusion ($kJkg^{-1}$)
m mass (kg)
P laser power (W)
Q rate of heat loss (or heat transfer rate) per unit area (Wm^{-2})
R_l laser-spot radius (m)
T temperature (K)
T_0 ambient temperature (K)
t time (s)
V volume (m^3)

Greek

η powder efficiency
ρ density (kgm^{-3})
λ thermal conductivity ($Wm^{-1}K^{-1}$)
γ absorption coefficient

Subscript

c clad
eff effective quantity
p powder
s substrate

REFERENCES

1. Nguyen Q., Yang C.Y., "Inverse determination of laser power on laser welding with a given width penetration by a modified Newton-Raphson method," *International Communications in Heat and Mass Transfer*, **65,** pp. 15-21 (2015).
2. Pavelic V., Tanbakuchi R., Uyehara O.A., "Experimental and computed temperature histories in gas tungsten arc welding of thin plates," *Welding Journal Research Supplement*, **48**, pp. 295-305 (1969).
3. Goldak J., Chakravarti A., Bibby M., "A new finite element model for welding heat sources," *Metallurgical and Material Transactions B*, **15B**, pp. 299-305 (1984).
4. Goldak J., "Computer modeling of heat flow in welds" *Metallurgical and Material Transactions B*, **17**, pp. 587-600 (1986).
5. Ha E.J., Kim W.S., "A study of low-power density laser welding process with evolution of free surface," *International Journal of Heat Fluid Flows*, **26 (4)**, pp. 613-521 (2005).
6. De A., DebRoy B., "Probing unknown welding parameters from convective heat transfer calculation and multivariable optimization," *Journal of Physics B*, **37 (1)**, pp. 140-150 (2004).
7. Lalas C., Tsirbas K., Salonitis K., Chryssolouris G., "An analytical model of the laser clad geometry," *International Journal of Advanced Manufacturing Technology*, **32**, pp. 34-41 (2007).
8. Toyserkani E., Khajepour A., Corbin S., "3-D finite element modeling of laser cladding by powder injection: effects of laser pulse shaping on the process," *Optics and Lasers in Engineering*, **41**, pp. 849-867 (2004).
9. Ya W., Pathiraj B., Liu S., "2D modeling of clad geometry and resulting thermal cycle during laser cladding," *Journal of Materials Processing Technology*, **230**, pp. 217-232 (2016).
10. Hofman J.T., de Lange D.E., Pathiraj B., Meijer J., "FEM modelling and experimental verification for dilution control in laser cladding," *Journal of Materials Processing Technology*, **211**, pp. 187-196 (2011).
11. Palumbo G., Pinto S., Tricarico L., "Numerical finite element investigation on laser cladding treatment of ring geometries," *Journal of Materials Processing Technology*, **155-156**, pp. 1443-1450 (2004).
12. Parekh R., Buddu R.K., Patel R.I., "Multiphysics simulation of laser cladding process to study the effect of process parameters on clad geometry," *Procedia Technology*, **23**, pp. 529-536 (2016).
13. Liu J., Li L., "Study on cross-section clad profile in coaxial single-pass cladding with a low-power laser," *Optics & Laser Technology*, **37**, pp. 478-482 (2005).
14. Sistaninia M., Sistaninia M., Moeanodini H., "Laser surface hardening considering coupled thermoelasticity," *Journal of Mechanics*, **25**, pp. 241-249 (2009).
15. Yang L.X., Peng X.F., Wang B.X., "Numerical modeling and experimental investigation on the characteristics of molten pool during laser processing," *International Journal of Heat and Mass Transfer*, **44**, pp. 4465-4473 (1986).
16 Lien F.S., Chen W.L., Leschziner M.A., "A multiblock implementation of a non-orthogonal, collocated finite volume algorithm for complex turbulent flows," *International Journal of Numerical Methods in Fluids*, **23**, pp. 567-588 (1996).

17. Mills K.C., "Recommended values of thermal physical properties for selected commercial alloys," *Woodhead Publishing Ltd*., Cambridge, UK (2002).
18. Hofman J.T., "Development of an observation and control system for industrial laser cladding," *Ph.D. Thesis*,University of Twente,The Netherlands (2009).

(Manuscript received December 24, 2018, accepted for publication May 24, 2019.)